Article

Vibronic and Cationic Features of 2-Fluorobenzonitrile and 3-Fluorobenzonitrile Studied by REMPI and MATI Spectroscopy and Franck-Condon Simulations

Shuxian Li [1], Yan Zhao [2,*], Yuechun Jiao [1,3], Jianming Zhao [1,3], Changyong Li [1,3,*] and Suotang Jia [1,3]

[1] State Key Laboratory of Quantum Optics and Quantum Optic Devices, Institute of Laser Spectroscopy, Shanxi University, Taiyuan, Shanxi, 030006, China
[2] Department of Physics and Electronics Engineering, Jinzhong University, Jinzhong, Shanxi 030619, China
[3] Collaborative Innovation Center of Extreme Optics, Shanxi University, Taiyuan, Shanxi, 030006, China.
* Correspondences: lichyongl@sxu.edu.cn, zhaoy@jzxy.edu.cn

Abstract: The fluorinated organic compounds have superior physicochemical properties than general organic compounds due to the strong C-F single bond, and widely used in medicine, biology, pesticides, and materials science. In order to gain a deeper understanding of the physicochemical properties of fluorinated organic compounds, fluorinated aromatic compounds have been investigated by various spectroscopic techniques. 2-Fluorobenzonitrile and 3-fluorobenzonitrile are important fine chemical intermediates, and their excited state S_1 and cationic ground state D_0 vibrational features remain unknown. In this paper, we used two-color resonance two photon ionization (2-color REMPI) and mass analyzed threshold ionization (MATI) spectroscopy to study S_1 and D_0 states vibrational features of 2-fluorobenzonitrile and 3-fluorobenzonitrile. The precise excitation energy (band origin) and adiabatic ionization energy were determined to be 36028 ± 2 cm^{-1} and 78650 ± 5 cm^{-1} for 2-fluorobenzonitrile; and 35989 ± 2 cm^{-1} and 78873 ± 5 cm^{-1} for 3-fluorobenzonitrile, respectively. The density functional theory (DFT) at the levels of RB3LYP/aug-cc-pvtz, TD-B3LYP/aug-cc-pvtz, and UB3LYP/aug-cc-pvtz were used to calculate the stable structures and vibrational frequencies for the ground states S_0, excited state S_1, and cationic ground state D_0, respectively. Franck-Condon spectral simulations for transitions of $S_1 \leftarrow S_0$ and $D_0 \leftarrow S_1$ were performed based on above DFT calculations. The theoretical and experimental results are in good agreement. The observed vibrational features in S_1 and D_0 states are assigned according to the simulated spectra and the comparison with structurally similar molecules. Several experimental findings and molecular features were discussed in detail.

Keywords: fluorobenzonitrile; vibronic spectroscopy; cationic spectroscopy; MATI; Franck-Condon simulation

1. Introduction

Due to the presence of the strong C-F single bond within the molecule, fluorinated organic compounds have superior physicochemical properties than general organic compounds, such as high thermal stability, high oxidative stability, weak intermolecular interaction and weak surface tension, which make them widely used in medicine, biology, pesticides, and materials science [1–5]. In recent years, in order to gain a deeper understanding of the physicochemical properties of fluorinated organic compounds, a large number of fluorinated aromatic compounds have been investigated by various spectroscopic techniques. In 2017, Ling et al. used femtosecond time-resolved photoelectron imaging to study the conformation of bi-fluorophenol and bi-fluoroaniline in the excited state S_1 after photoexcitation [6,7]. Wijngaarden's group used high-resolution microwave spectroscopy to measure the rotation spectra of fluorine substituted benzaldehyde, benzonitrile, phenol, and pyridine derivatives to study the molecular structure changes caused by fluorination and intramolecular hydrogen bonding interactions [8–10]. Many

Preprints (www.preprints.org) | NOT PEER-REVIEWED | Posted: 29 May 2023 doi:10.20944/preprints202305.2016.v1

experimental groups have also studied the vibrational spectra of excited state S_1 and cationic ground state D_0 of fluorine substituted phenol, anisole, and aniline derivatives using laser-induced fluorescence (LIF), resonance-enhanced multiphoton ionization (REMPI), and mass analyzed threshold ionization (MATI) spectroscopy [11–14]. Mono-fluorobenzonitrile is a very important class of intermediate for organic synthesis, and their vibrational and rotational properties have been reported in many studies [15–18]. Kamaee et al. investigated the structural trends in mono-, di-, and pentafluorobenzonitriles using Fourier transform microwave spectroscopy [10]. Palmer et al. measured photoelectron spectroscopy of 2-fluorobenzonitrile (2FBN) and 3-fluorobenzonitrile (3FBN), and reported the ionization energies (IE) of 9.78 eV and 9.79 eV, respectively [19]. Jiang and Levy used laser induced fluorescence and dispersive fluorescence spectroscopy to study the vibrational relaxation of the excited state of 4-fluorobenzonitrile (4FBN) molecule [20]. In 2018, Zhao et al. [21] studied the vibrational features of the excited and cationic ground states of 4FBN by REMPI and MATI techniques. Silva et al. [16] measured the UV-Vis spectra of monofluorobenzonitriles in dichloromethane, and from the curves they measured, the approximate origins of 2FBN and 3FBN can be estimated at 283 nm. To the best of our knowledge, the vibrational properties of the excited states and cationic ground states of 2FBN and 3FBN have not been reported in the literature.

MATI and zero kinetic energy (ZEKE) spectroscopy are currently the most popular high-resolution techniques for measuring vibrational features of cationic ground states. ZEKE spectroscopy detects the electrons and MATI detects the ions yielded by field ionization of Rydberg neutrals. Due to the different masses of various ions, MATI spectroscopy has the ability of eliminating impurity interference. Kwon's group built a vacuum ultraviolet single photon MATI system to study many cationic vibrational features [22–29]. Tzeng's group and Ketkov's group used two-color MATI to study the cationic spectra of many benzene derivatives and sandwich molecules [30–36]. Wright's group used ZEKE technology to research cationic vibrational features of many halogenated benzene and their derivatives [37–42]. In this paper we used two-color REMPI and MATI techniques to study the vibrational features of the excited states and cationic ground states of 2FBN and 3FBN. The precise excitation energies and adiabatic ionization energies were determined. The measured vibrational features were assigned, and several experimental findings are analyzed and discussed in detail.

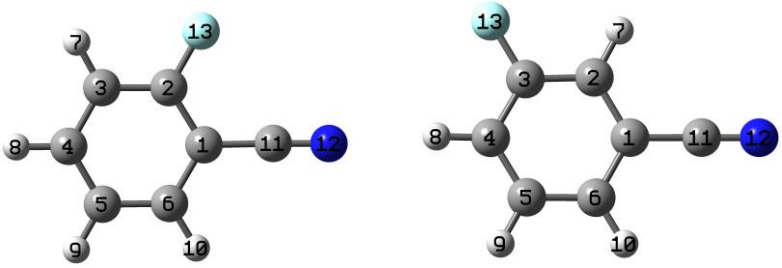

Figure 1. The stable structures of 2- and 3-fluorobenzonitrile with atomic labels.

2. Results

The stable structures of 2- and 3-fluorobenzonitrile with atomic labels are shown in Figure 1. 2FBN and 3FBN molecules consist of 13 atoms with a total of 33 normal vibrational modes, 30 modes of which are at aromatic ring and 3 modes at CN group. The labeling convention of the vibrational modes follows the Varsanyi's system [43]. Vibronic transitions are expressed in the Wilson notation based on benzene modes, where the v'←v" transition in the normal mode n is represented by $n_{v''}^{v'}$ [44], and subscript V" is omitted in present research as it is a constant 0 (The low energy level of the transition is the vibrationless or zero point energy level of the low electronic state).

2.1. Vibronic Features of 2-Fluorobenzonitrile in the S_1 State

Preprints (www.preprints.org) | NOT PEER-REVIEWED | Posted: 29 May 2023 doi:10.20944/preprints202305.2016.v1

The vibronic spectrum of the $S_1 \leftarrow S_0$ transition of 2FBN was measured by two-color REMPI experiment with the vibration frequency range of 0 – 1350 cm^{-1}. The experimental result is shown in Figure 2a, and its Franck-Condon simulation calculated at B3LYP/aug-cc-pvtz level is shown in Figure 2b. It can be seen that the experimental result is in good agreement with the calculated one. The obvious feature of both REMPI and its simulation in Figure 2 is that the rate of signal-to-noise in low frequency region is greater than that in high frequency region. The simulation spectrum shows that the bands in high frequency region are dense, and consist of many fundamentals, overtones, and combinations of various modes, many of which are very weak. So, dense and weak bands raise the spectral baseline and result in a bad rate of signal-to-noise in high frequency region. The band at certain frequency in the spectrum maybe come from several component (or vibration mode) contributions. For simplicity's sake, we only list the largest contributor in Table 1.

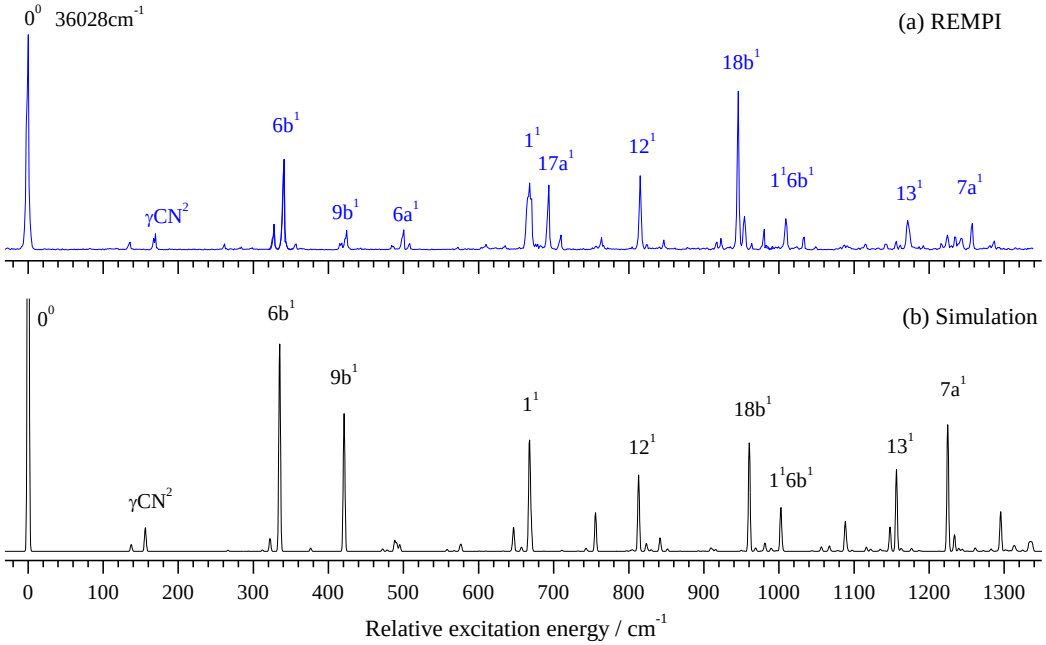

Figure 2. REMPI spectrum of 2-fluorobenzonitrile (a) and its Franck-Condon simulation (b).

Based on DFT calculation and spectral simulation, we analyzed and assigned the vibronic spectra of 2FBN. It is very clear in Figure 2a that the band at 36028 cm^{-1} is assigned to the band origin of the $S_1 \leftarrow S_0$ transition. Many in-plane vibrational modes of the ring are active, and most of them are very strong in the REMPI spectrum. The bands at 136, 341, 424, 500, 668, 815, 946, 1171, and 1257 cm^{-1} are assigned to fundamental modes 15, 6b, 9b, 6a, 1, 12, 18b, 13, and 7a, respectively. One out-of-plane fundamental mode at the ring was observed, which appeared at 693 cm^{-1}, and assigned to mode 17a. Several overtone vibrations were observed, which appeared at 170, 635, and 846 cm^{-1}, and assigned to γCN^2, $16b^2$, and $9b^2$, respectively. Other bands observed in REMPI spectrum are assigned to the combined vibrations of several modes. All the measured vibrational frequencies, calculated frequencies, and possible assignments are listed in Table 1.

From measured REMPI spectra in Figure 2a, we can find that the vibronic band 1^1 is much wider than other bands. From simulation calculation we knew that the band 1^1 consists of three components: $16a^1 10a^1$ (665.2 cm^{-1}), 1^1 (667.5 cm^{-1}), and $6b^2$ (669.7 cm^{-1}). The calculated dipole strength at the level of TD-B3LYP/aug-cc-pvtz for these three components are 3.365E-5, 1.254E-2, and 3.2E-3, respectively. Due to the very close vibrational energy, the resonance interactions may have played a role in the broadening of the experimental spectral line.

Table 1. Observed bands in the vibronic spectrum of 2FBN and their possible assignments [a].

Preprints (www.preprints.org) | NOT PEER-REVIEWED | Posted: 29 May 2023 doi:10.20944/preprints202305.2016.v1

Transition energy (cm^{-1})	Relative intensity	Shift (cm^{-1})	Calc. (cm^{-1})	Assignment [b]
36028	100	0	0	0^0
36164	4	136	137	15^1
36198	7	170	156	γCN^2
36290	3	262		$10b^1\gamma CN^1$
36356	12	328		$10a^1\gamma CN^1$
36369	42	341	335	$6b^1$
36452	9	424	421	$9b^1$
36528	9	500	495	$6a^1$
36638	3	610		$16a^110b^1$
36663	31	635	646	$16b^2$
36696	30	668	668	1^1
36721	30	693	698	$17a^1$
36738	7	710	711	$6b^110b^2$
36792	6	764	755	$9b^16b^1$
36843	34	815	813	12^1
36874	2	846	841	$9b^2$
36945	4	917	910	βCN^16b^1
36950	5	922	916	$6a^19b^1$
36974	74	946	960	$18b^1$
36982	15	954	969	$12^1\gamma CN^2$
37008	10	980	981	$6b^116b^2$
37037	14	1009	1003	1^16b^1
37062	6	1034	1022	$16b^210b^2$
37199	14	1171	1156	13^1
37285	12	1257	1224	$7a^1$
37315	4	1287	1295	$18b^16b^1$

[a] Experimental values are shifts from 36028 cm^{-1}, and the calculated ones (scaled by 0.9649) are obtained from the TD-B3LYP/aug-cc-pvtz calculations. [b] β, in-plane bending; γ, out-of-plane bending.

2.2. Photoionization Efficiency (PIE) Spectra of 2FBN

In order to measure the cationic spectra, we require first to know the ionization energy (IE). With the present experimental setup, the IE can be measured by photoionization efficiency (PIE) or MATI experiments. The PIE approach detects the prompt ions involving the field-ionization of high n Rydberg neutrals, and yield a strong signal to leads to an abruptly rising step near the ionization limit. In contrast, the MATI spectrum detects the threshold ions and yields a sharp peak at the ionization threshold and vibrational features of the cation. We have recorded both the PIE and MATI spectra by scanning the frequency of the ionization laser over a large range to determine the IE of 2FBN. Figure 3a and 3b show the PIE and MATI spectra via the intermediate state S_10^0 (36028 cm^{-1}). The adiabatic IE of 2FBN was determined to be 78647 ± 10 cm^{-1} by PIE and 78650 ± 5 cm^{-1} (9.7514 ± 0.0006 eV) by MATI including the correction of Stark effect, respectively. These results are in good agreement with the previous measured value of 9.78 eV (78881 cm^{-1}) [19] by photoelectron spectroscopy with He I UV-light source.

Preprints (www.preprints.org) | NOT PEER-REVIEWED | Posted: 29 May 2023 doi:10.20944/preprints202305.2016.v1

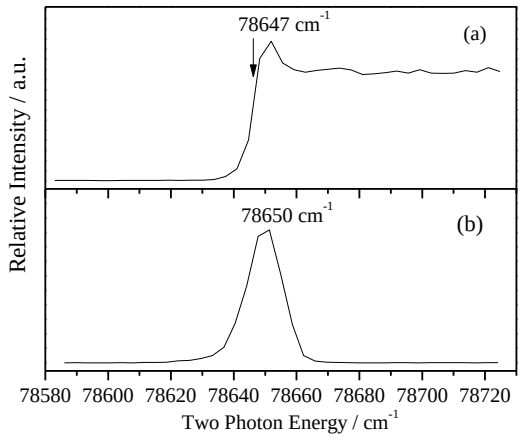

Figure 3. PIE spectrum of 2-fluorobenzonitrile recorded by ionizing via $S_1 0^0$ intermediate state at 36028 cm^{-1} (a) and MATI spectrum near the cationic origin 0^+ for comparison (b).

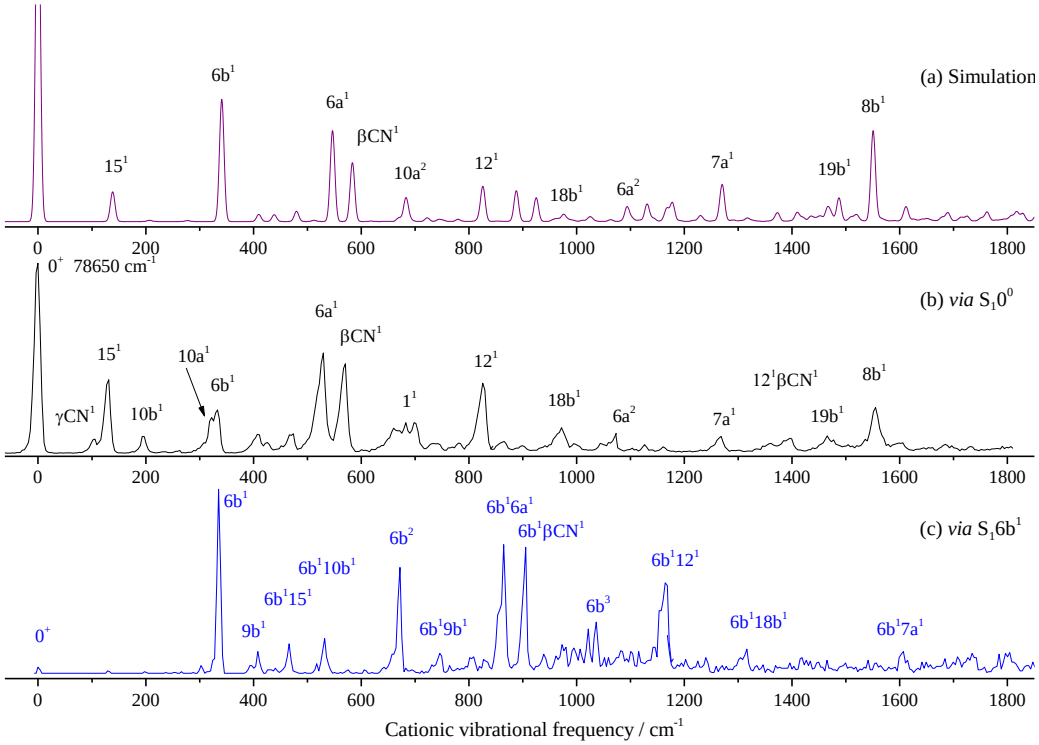

Figure 4 Franck-Condon simulation of the $D_0 \leftarrow S_1 0^0$ transition (a) and the MATI spectra of 2-fluorobenzonitrile *via* $S_1 0^0$ (b) and $S_1 6b^1$ (c) intermediate states.

2.3. Cationic Spectra of 2FBN

To investigate the molecular geometry and vibrational features of the 2FBN cation, the MATI spectra were recorded by ionizing via the $S_1 0^0$, $S_1 6b^1$ ($0^0 + 341 cm^{-1}$), $S_1 11^1$ ($0^0 + 668$ cm^{-1}), $S_1 12^1$ ($0^0 + 815$ cm^{-1}), and $S_1 18b^1$ ($0^0 + 946$ cm^{-1}) intermediate states.

We first performed the theoretical calculation and spectral simulation. The Franck-Condon simulation is shown in Figure 4a, and the corresponding MATI spectrum via $S_1 0^0$ is shown in Figure 4b. From Figure 4a and 4b we know that the theoretical and experimental spectra are in good agreement. The most intense peak corresponds to the origin of the $D_0 \leftarrow S_1$ transition of 2FBN. Spectral features were assigned, mainly based on DFT calculations, Franck-Condon simulation, and comparisons with the available data on substituted benzonitriles. Spectral assignment is a very tedious and error prone thing. Accurate assignments can be obtained by high dimensional or even full dimensional vibrational calculations [45,46]. For the present work, we use the Franck-Condon simulation, which greatly facilitates spectral identification work. The bands at 131, 333, 530, 571, 683,

Preprints (www.preprints.org) | NOT PEER-REVIEWED | Posted: 29 May 2023 doi:10.20944/preprints202305.2016.v1

826, 972, 1268, and 1555 cm^{-1} are relatively intense and assigned to ring or CN group in-plane motion modes 15, 6b, 6a, βCN, 1, 12, 18b, 7a, and 8b, respectively. Several out-of-plane bending vibrations were also observed, such as γCN and 10b appearing at 106 and 197 cm^{-1}, respectively. Other bands are weak and assigned to overtone or combination vibrations. The measured and calculated cationic vibrational frequencies, and their possible assignments are listed in Table 2.

In order to find more vibrational modes of 2FBN cation, the different intermediate states were used to record MATI spectra. Figure 4c shows the MATI spectra *via* $S_1 6b^1$ (0^0 + 341cm^{-1}). Comparing with Figure 4b, we can find that when $S_1 6b^1$ is used as the intermediate state, most of spectral features can be assigned to combinations of 6b and the modes found in MATI via $S_1 0^0$. This can be verified by shifting Figure 4c to the left to align its band 6b with the 0^+ band in Figure 4b. No more fundamental modes than the MATI via $S_1 0^0$ are found.

Figure 5 shows the MATI spectra via the intermediate states of $S_1 1^1$ (0^0 + 668 cm^{-1}), $S_1 12^1$ (0^0 + 815 cm^{-1}), and $S_1 18b^1$ (0^0 + 946 cm^{-1}). Similarly, when $S_1 1^1$ (0^0 + 668 cm^{-1}) was used as the intermedia state, a lot of bands are assigned to the combination vibrations of the mode 1 and those found in MATI via $S_1 0^0$. In the lower frequency region, substituent CN out-of-plane bending γCN and its overtone γCN^2 were found. Aromatic ring out-of-plane bending 10a and its overtone $10a^2$ were also observed. Other bands are weak and assigned to combination vibrations of several modes.

Similarly, when $S_1 12^1$ is used as the intermediate, as shown in Figure 5b, except for the bands at 1064 and 1646 cm^{-1} being assigned to $6a^2$ and 12^2, other bands greater than 823 cm^{-1} ($D_0 12^1$) are assigned to combinations of 12^1 and other modes. In lower frequency region, some fundamental modes are active, which have been found in the MATI spectrum via $S_1 0^0$ or $S_1 1^1$. For the MATI via $S_1 18b^1$ in Figure 5c, the spectral feature is similar to the MATI via $S_1 12^1$, and all the assignments as well as the calculated and measured values are listed in Table 2.

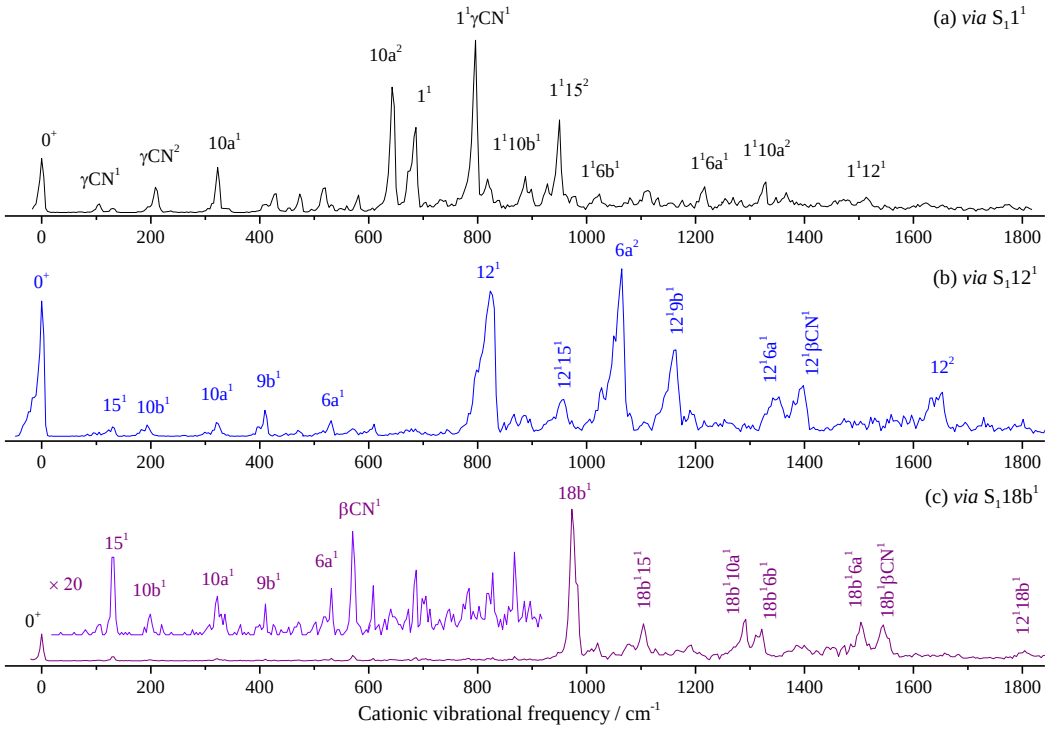

Figure 5. MATI spectra of 2-fluorobenzonitrile *via* $S_1 1^1$ (a), $S_1 12^1$ (b), and $S_1 18b^1$ intermediate states.

Table 2. Assignment of the observed bands (cm^{-1}) in the MATI spectra of 2FBN. [a]

Preprints (www.preprints.org) | NOT PEER-REVIEWED | Posted: 29 May 2023 doi:10.20944/preprints202305.2016.v1

Intermediate levels in the S_1 state					Calc.	Assignment [b]
0^0	$6b^1$	1^1	12^1	$18b^1$		
106		106			104	γCN^1
131			130	132	139	15^1
197			193	199	205	$10b^1$
		209				γCN^2
		323	321	322	335	$10a^1$
333	335				341	$6b^1$
407	408		409	410	410	$9b^1$
		430				$6b^1\gamma CN^1$
	466					$6b^115^1$
474		473				$15^2\gamma CN^2$
		520				$10a^110b^1$
530			531	532	547	$6a^1$
	532					$6b^110b^1$
		582				$6b^115^1\gamma CN^1$
		643				$10a^2$
571			570	571	584	βCN^1
	672	672				$6b^2$
683		687		687	696	1^1
698						$16a^110b^1$
	746					$6b^19b^1$
		796				$1^1\gamma CN^1$
		818				1^115^1
826			823		826	12^1
	865					$6b^16a^1$
		888				1^110b^1
	906					$6b^1\beta CN^1$
		950				1^115^2
			955			12^115^1
972				973	976	$18b^1$
		1023				1^16b^1
	1036					$6b^3$
1059			1064			$6a^2$
				1104		$18b^115^1$
	1164		1160			$6b^112^1$
		1217				1^16a^1
1268					1271	$7a^1$
				1292		$18b^110a^1$
	1316			1321		$6b^118b^1$
		1329				1^110a^2
			1349			12^16a^1
			1394			$12^1\beta CN^1$
1396					1410	$12^1\beta CN^1$
1466					1466	$19b^1$
				1503		$18b^16a^1$
		1513				1^112^1
				1545		$18b^1\beta CN^1$
1555					1551	$8b^1$
	1607					$6b^17a^1$
			1646			12^2

[a] The experimental values are shifts from 78650 cm^{-1}, whereas the calculated ones are obtained from the B3LYP/aug-cc-pVDZ calculations, scaled by 0.9849. [b] β, in-plane bending; γ, out-of-plane bending.

2.4. Vibronic Features of 3-Fluorobenznitrile in the S_1 State

Preprints (www.preprints.org) | NOT PEER-REVIEWED | Posted: 29 May 2023 doi:10.20944/preprints202305.2016.v1

The vibronic spectrum in the S_1 state of 3FBN is shown in Figure 6a together with its Franck-Condon simulation shown in Figure 6b for comparing. The entire simulated spectra appear comparable to the 2-color REMPI spectra in Figure 6a. The distinct band corresponding to the transition energy of 35989 cm^{-1} is identified as the origin of the $S_1 \leftarrow S_0$ electronic transition. Table 3 lists the observed vibronic transition energies along with the energy shifts with respect to the band origin, band relative intensities, and possible assignments. The spectral assignment of 3FBN was accomplished by comparing with those of 4-fluorobenzonitrile, 3-fluorophenol, TD-B3LYP/aug-cc-pvtz calculation, and Franck-Condon simulation. The spectral features in Figure 6a mainly result from vibronic transitions related to the in-plane ring deformation and substituent sensitive bending vibrations. The bands appeared at 140, 385, 401, 470, 560, 660, 958, 1147, 1271, and 1374 cm^{-1} are assigned to in-plane stretching or bending vibrations 15, 9a, 6b, 6a, βCN, 1, 12, 9b, 13, and 19a, respectively. The out-of-plane overtone vibrations $\gamma(CN)^2$ and $10b^2$ are also observed in lower frequency region. Other bands are assigned to combination vibrations of several modes.

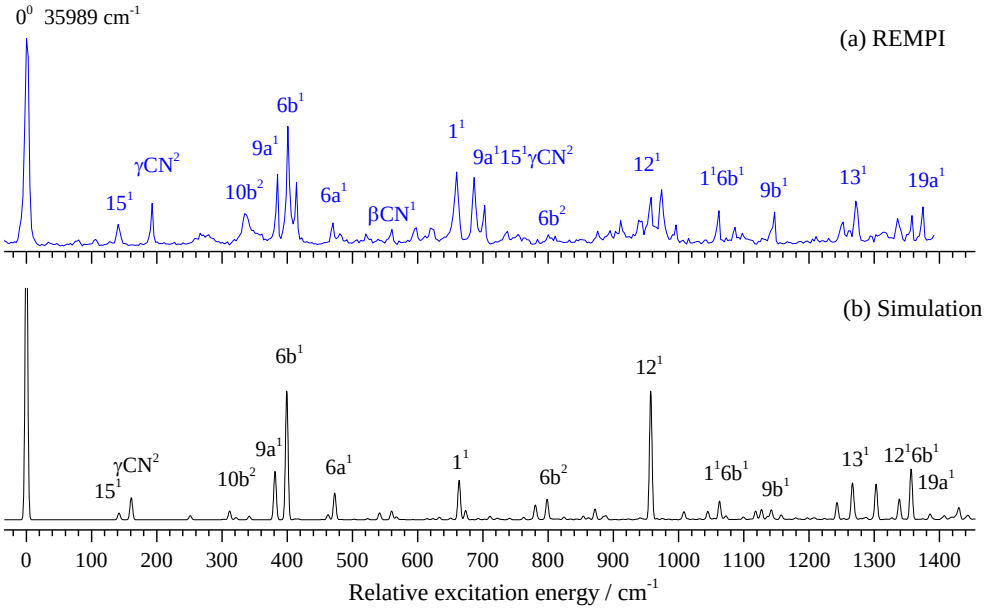

Figure 6. REMPI spectrum of 3-fluorobenzonitrile (a) and its Franck-Condon simulation (b).

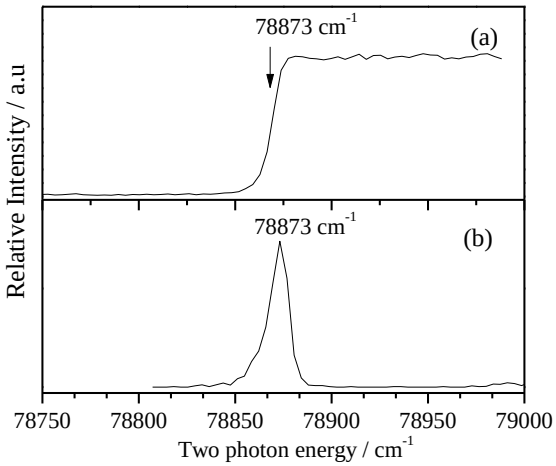

Figure 7. PIE spectrum of 3-fluorobenzonitrile recorded by ionizing via its $S_1 0^0$ state at 35989 cm^{-1} (a) and MATI spectrum near the cationic origin 0^+ for comparison (b).

2.5. PIE Spectra of 3FBN

Preprints (www.preprints.org) | NOT PEER-REVIEWED | Posted: 29 May 2023 doi:10.20944/preprints202305.2016.v1

Similar to the 2FBN, ionization energy is very important for the cationic spectral measurements. We first performed the PIE experiment to determine the IE of 3FBN to be 78873 ± 10 cm^{-1}, and then measured the MATI spectra to give the precise IE of 3FBN to be 78873 ± 5 cm^{-1}. The PIE and MATI spectra via $S_1 0^0$ are shown in Figure 7a and 7b for comparing. It is obvious that they are very consistent.

Table 3. Assignment of observed bands (cm^{-1}) in the 2-color REMPI spectrum of 3FBN. [a]

Transition energy	Exp.	Relative Intensity	Calc. [a]	Assignment [b]
35989	0	100		0^0, band origin
36129	140	11	142	15^1
36182	193	21	171	$\gamma(CN)^2$
36255	266	7	251	$10b^1\gamma(CN)^1$
36324	335	16	342	$10b^2$
36374	385	35	381	$9a^1$, β(C-F)
36390	401	58	399	$6b^1$, β(CCC)
36403	414	31	417	$10b^1\gamma(CN)^3$
36459	470	11	473	$6a^1$, β(CCC)
36469	480	6	484	$10b^215^1$
36509	520	6	523	$9a^115^1$
36549	560	9	567	βCN
36584	595	9	593	$10b^3\gamma(CN)^1$
36611	622	9	623	$10a^2\gamma(CN)^2$
36649	660	36	663	1^1, breather
36675	686	33	684	$9a^115^1\gamma(CN)^2$
36692	703	20	709	$15^1\beta(CN)^1$
36727	738	8	741	$6b^110b^2$
36789	800	6	798	$6b^2$
36864	875	8	872	$6a^16b^1$
36900	911	13	915	$1^110b^1\gamma(CN)^1$
36927	938	13	940	$6b^215^1$
36947	958	24	957	12^1
36963	974	27	975	$1^110a^1\gamma(CN)^1$
36985	996	11	996	$6a^19a^115^1$
37051	1062	17	1063	1^16b^1
37075	1086	9	1087	$4^16a^1\gamma(CN)^1$
37136	1147	17	1142	$9b^1$
37241	1252	12	1253	$6a^16b^19a^1$
37260	1271	22	1266	13^1
37304	1315	7	1314	$11^16b^116b^1$
37324	1335	14	1338	12^19a^1
37347	1358	15	1356	12^16b^1
37363	1374	19	1385	$19a^1$

[a] The experimental values are shifts from 35989 cm^{-1}, whereas the calculated ones are obtained from the TD-B3LYP/aug-cc-pVDZ calculations, scaled by 0.9722. [b] β, in-plane bending; γ, out-of-plane bending.

2.6. MATI Spectra of 3FBN

Preprints (www.preprints.org) | NOT PEER-REVIEWED | Posted: 29 May 2023 doi:10.20944/preprints202305.2016.v1

Figures 8a and 8b show the calculated Franck-Condon spectrum and measured MATI spectrum via $S_1 0^0$ state at 35989 cm^{-1}, respectively. We can see that they are in good agreement. Many in-plane vibrations are active, such as modes 15, 6b, 6a, 1, 12, 18a, 9b, 18b, 13, and 8a appearing at 133, 371, 498, 668, 978, 1066, 1117, 1144, 1307, and 1566 cm^{-1}, respectively. Out-of-plane bending modes 10b and 10a are also observed, but they are weak. Other bands are assigned to combinations of several modes. All the experimental and calculated cationic vibrational frequencies of 3FBN and corresponding assignments are listed in Table 4.

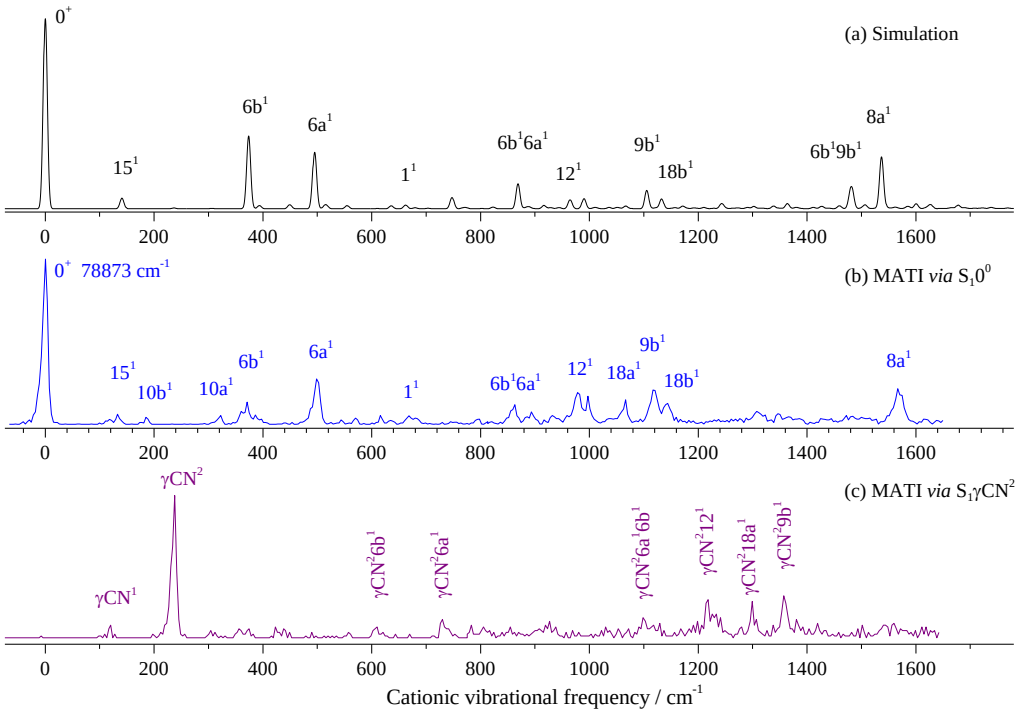

Figure 8. Franck-Condon simulation of the transition $D_0 \leftarrow S_1 0^0$ (a) and the MATI spectra of 3-fluorobenzonitrile *via* $S_1 0^0$ (b) and $S_1 \gamma CN^2$ (c) intermediate states.

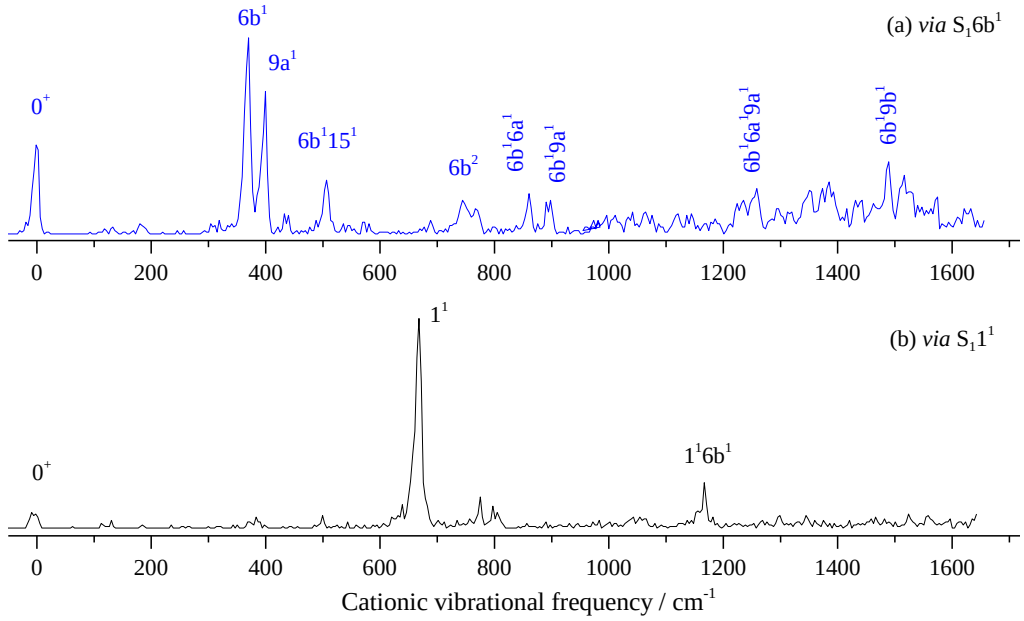

Figure 9. The MATI spectra of 3-fluorobenzonitrile *via* $S_1 6b^1$ (a) and $S_1 1^1$ (b) intermediate states.

Table 4. Assignment of observed bands (in cm^{-1}) in the MATI spectra of 3FBN. [a]

Preprints (www.preprints.org) | NOT PEER-REVIEWED | Posted: 29 May 2023 doi:10.20944/preprints202305.2016.v1

Intermediate levels in the S_1 state				Calc.	Assignment [b]
0^0	$\gamma(CN)^2$	$6b^1$	1^1		
	120			118	$\gamma(CN)^1$
133				141	15^1
	238			237	$\gamma(CN)^2$
185				188	$10b^1$
322				331	$10a^1$
371		370		374	$6b^1$, β(CCC)
		399		394	$9a^1$
498				495	$6a^1$, β(CCC)
		506			$6b^115^1$
	609				$\gamma(CN)^26b^1$
615				605	$16a^1$
668			668	679	1^1, breathing
		688			$6b^110b^115^1$
	730				$\gamma(CN)^26a^1$
		744			$6b^2$
			775		4^110b^1
			803		1^115^1
863		860			$6b^16a^1$
893		894			$6a^19a^1$
978				965	12^1, β(CCC)
997				990	$6a^2$
1066				1067	$18a^1$, β(CH)
	1098				$\gamma(CN)^26a^16b^1$
1117				1105	$9b^1$, β(CH)
1144				1133	$18b^1$, β(CH)
			1166		1^16b^1
	1218				$\gamma(CN)^212^1$
		1235			$6b^26a^1$
		1258			$6b^16a^19a^1$
	1299				$\gamma(CN)^218a^1$
1307				1302	13^1, β(CH)
		1350			$6b^112^1$
	1357				$\gamma(CN)^29b^1$
		1374			$6b^16a^2$
		1385		1382	$19a^1$
		1489			$6b^19b^1$
1566				1537	$8a^1$, ν(CC)
		1516			$6b^118b^1$
		1574			$6b^118a^115^1$

[a] The experimental values are shifts from 78873 cm^{-1}, whereas the calculated ones are obtained from the B3LYP/aug-cc-pVDZ calculations, scaled by 0.9704. [b] β, in-plane bending; γ, out-of-plane bending.

When measuring the MATI via $S_1\gamma CN^2$ (Figure 8c), the distinct feature at 238 cm^{-1} is assigned to $D_0\gamma CN^2$, which follows the propensity rule $\Delta v = 0$. The fundamental vibration γCN^1 was also observed at 120 cm^{-1} with a weak intensity, which did not appear in the REMPI spectrum. Other bands are assigned to combination vibrations of γCN^2 and fundamental vibrations.

When measuring the MATI via S_16b^1, as shown in Figure 9a, the distinct feature at 370 cm^{-1} is assigned to D_06b^1, which follows the propensity rule $\Delta v = 0$. The intense band at 399 cm^{-1} is assigned to $9a^1$. Other bands are assigned to combination vibrations of $6b^1$ and fundamental vibrations. Figure 9b shows the MATI spectrum via S_11^1, where the

Preprints (www.preprints.org) | NOT PEER-REVIEWED | Posted: 29 May 2023 doi:10.20944/preprints202305.2016.v1

cationic vibration 1^1 (668 cm^{-1}) is most intense. The bands at 775, 803, and 1166 cm^{-1} are assigned to combination vibrations $4^1 10b^1$, $1^1 15^1$, and $1^1 6b^1$, respectively.

3. Discussion

3.1 Breathing Vibrational Band of 2FBN

Whether the vibrational spectra of excited state S_1 or cationic ground state D_0, the frequencies of different vibrations in the high-frequency region maybe very close or even the same, which may come from the fundamental, overtone or combination vibrations. For example, the breathing vibration 1^1 of 2FBN in the REMPI spectrum (see Figure 2a) appears at 668 cm^{-1}. The theoretical calculation shows that there are also two weaker vibrations $16a^1 10a^1$ and $6b^2$, whose vibrational frequencies are close to that of mode 1^1. The calculated vibration frequencies of $16a^1 10a^1$, 1^1 and $6b^2$ are 665.2 cm^{-1}, 667.5 cm^{-1} and 669.7 cm^{-1}, respectively. They are so close that the spaces between them are less than the experimental resolution, which leads to a wide spectral band in the REMPI spectrum. When using this band as the intermediate state to perform the MATI experiment, according to the propensity rule of $\Delta v = 0$, these three vibrational modes of cation may be observed with great intensity. Generally, the vibration frequency of cation is slightly different from that of the excited state for the same vibrational mode, and the frequency change can be not consistent for various vibration modes. So, these three vibration modes of cation of 2FBN may be separated in the MATI spectrum. As shown in Figure 5a, the cationic mode 1^1 appeared at 687 cm^{-1}, $6b^2$ appeared at 672 cm^{-1}, and $10a^1$ and $10a^2$ were also observed at 322.7 and 643.2 cm^{-1}, respectively. The strength of the MATI signal is not only related to the Franck-Condon factor, but also to the population of the intermediate state S_1, and further related to the resonance degree of each vibration mode with the excitation ($S_1 \leftarrow S_0$) photon frequency. The experimental results demonstrate that the superposition band of several vibrations can be used as an intermediate state to do the MATI experiments, and more vibrational modes of cation can be observed.

3.2. Molecular Structure in S_0, S_1, and D_0 States and Vibrational Frequencies

Theoretical calculations show that the stable configurations of the ground state S_0, excited state S_1, and cationic ground state D_0 of 2FBN and 3FBN molecules all have Cs symmetry, and all the atoms are in the ring plane. This is consistent with their large Franck-Condon factors, intense REMPI and MATI signals, and MATI spectra following the propensity rule of $\Delta v = 0$. However, in the transitions of $S_1 \leftarrow S_0$ and $D_0 \leftarrow S_1$, the bond length and bond angle of molecules have changed slightly. Table 5 and Table 6 show the bond lengths and bond angles of the S_0, S_1, and D_0 states of 2FBN and 3FBN calculated at levels of RB3LYP/ang-cc-pvtz, TD-B3LYP/ang-cc -pvtz, and UB3LYP/ang-cc-pvtz, respectively. It can be seen that the bond lengths between adjacent carbon atoms of the ring of 2FBN are very close to the corresponding bond lengths of 3FBN. After the transition of $S_1 \leftarrow S_0$, each C-C bond length increased, resulting in the perimeters of ring of 2FBN and 3FBN increased by 0.160 Å and 0.158 Å, respectively. The transition of $D_0 \leftarrow S_1$ leads to the shortening of four C-C bonds and lengthening of two C-C bonds. The overall effect of $D_0 \leftarrow S_1$ transition is that the perimeters of ring of 2FBN and 3FBN decrease by 0.073 Å and 0.072 Å, respectively. Further, the ring C-C bond lengths of D_0 state is averagely larger than that of S_0 state. The perimeters of the aromatic ring of 2FBN and 3FBN at the cationic ground states are 0.087 Å and 0.086 Å larger than those of the neutral ground state S_0, respectively. That is, the perimeters or average bond lengths of the ring in the ground state S_0, excited state S_1, and cationic ground state D_0 meet the relationship: $S_0 < D_0 < S_1$. The length of a chemical bond reflects, to some extent, the strength of that bond. The greater the bond length, the weaker the bond strength. The frequency of an ideal oscillator is proportional to the square root of the bond strength, so the larger the bond length, the lower the vibration frequency. On this basis, we can predict that, on average, the vibration frequencies of the ground state S_0, the excited state S_1 and the cationic ground state D_0

Preprints (www.preprints.org) | NOT PEER-REVIEWED | Posted: 29 May 2023 doi:10.20944/preprints202305.2016.v1

meet the relationship: $S_0 > D_0 > S_1$. The 33 normal vibration frequencies calculated at the B3LYP/ang-cc-pvtz level of 3FBN were statistically analyzed. On average, the vibration mode frequency of the ground state S_0 is about 21 cm^{-1} greater than that of the cationic ground state D_0, and the vibration frequency of D_0 is about 43 cm^{-1} greater than that of S_1. For example, the frequencies of breathing vibration mode 1 for S_0, D_0, and S_1 of 2FBN measured in the experiment are 724 [18], 685, and 668 cm^{-1}, respectively; for the mode 12 are 835 [18], 823, and 815 cm^{-1}, respectively, and for the mode 18b are 1100 [18], 973, and 946 cm^{-1}, respectively. The reported experimental and theoretical data of mFBT and mDFB [47] also indicate that most of the vibrational modes of these two molecules also follow this rule. Furthermore, from above vibration data we know that the frequency variation is larger for out-of-plane mode (such as 18b of 2FBN) than for in-plane mode (such as modes 1 and 12 of 2FBN). Our DFT theoretical results show that this law holds for most vibration modes of benzene derivative.

Table 5. Bond length and bond angle of electronic ground state S_0, first excited state S_1 and cationic ground state D_0 of 2-fluorobenzonitrile calculated at B3LYP/aug-cc-pvtz level.

	S_0	S_1	D_0	$\Delta(S_1-S_0)$	$\Delta(D_0-S_1)$	$\Delta(D_0-S_0)$
Bond length (Å)						
C1-C2	1.396	1.436	1.455	0.040	0.019	0.059
C2-C3	1.381	1.406	1.393	0.025	-0.013	0.012
C3-C4	1.389	1.409	1.372	0.020	-0.037	-0.017
C4-C5	1.392	1.408	1.434	0.016	0.026	0.042
C5-C6	1.385	1.421	1.386	0.036	-0.035	0.001
C6-C1	1.401	1.424	1.391	0.023	-0.033	-0.010
C1-C11	1.427	1.395	1.407	-0.032	0.012	-0.020
C11-N12	1.152	1.165	1.158	0.013	-0.007	0.006
C2-F13	1.341	1.324	1.296	-0.017	-0.028	-0.045
Band angle (°)						
C1-C2-C3	122.0	124.7	122.5	2.7	-2.2	0.5
C2-C3-C4	118.8	119.0	117.5	0.2	-1.5	-1.3
C3-C4-C5	120.5	118.1	121.1	-2.4	3.0	0.6
C4-C5-C6	120.0	122.7	121.4	2.7	-1.3	1.4
C5-C6-C1	120.4	120.6	119.0	0.2	-1.6	-1.4
C6-C1-C2	118.3	114.9	118.4	-3.4	3.5	0.1

For 2FBN and 3FBN, the bond lengths of C-N in S_0 state are equal (1.152 **Å**), also equal in S_1 state (1.165 **Å**), and almost equal in D_0 state (1.158 and 1.155 **Å**). This means that the CN bond is very strong and did not changed with substitution position (*ortho*- or *meta*-). The CF bond length yields slight change with different substitution positions.

Aromatic ring includes six bond angles of C-C-C. In the electronic transition, the bond angle of the ring also undergoes a certain degree of change. Four angles have a variation of approximately 2-3 °, and other two have relatively small changes. In the transitions of $S_1 \leftarrow S_0$ and $D_0 \leftarrow S_1$, variations of the bond angle and bond length of rings lead to the ring expansion and contraction, further activating a large number of in-plane vibration modes. Most of the observed vibronic features in experiments were assigned to in-plane vibrations, only a few of out-of-plane modes were observed. Many benzene derivative molecules exhibit such characteristics [48–53].

Table 6. Bond length and bond angle of the electronic ground state S_0, first excited state S_1 and cationic ground state D_0 of 3-fluorobenzonitrile calculated at B3LYP/aug-cc-pvtz level.

Preprints (www.preprints.org) | NOT PEER-REVIEWED | Posted: 29 May 2023 doi:10.20944/preprints202305.2016.v1

	S_0	S_1	D_0	$\Delta(S_1-S_0)$	$\Delta(D_0-S_1)$	$\Delta(D_0-S_0)$
Bond length (Å)						
C1-C2	1.398	1.425	1.380	0.026	-0.045	-0.018
C2-C3	1.380	1.413	1.393	0.033	-0.019	0.013
C3-C4	1.384	1.406	1.433	0.022	0.027	0.049
C4-C5	1.390	1.404	1.374	0.014	-0.029	-0.016
C5-C6	1.387	1.411	1.395	0.024	-0.016	0.008
C6-C1	1.398	1.438	1.449	0.039	0.010	0.051
C1-C11	1.430	1.397	1.415	-0.033	0.017	-0.015
C11-N12	1.152	1.165	1.155	0.013	-0.009	0.003
C2-F13	1.346	1.330	1.300	-0.016	-0.030	-0.046
Band angle (°)						
C1-C2-C3	118.2	118.4	116.9	0.2	-1.4	-1.3
C2-C3-C4	122.5	125.2	123.4	2.7	-1.7	0.9
C3-C4-C5	118.5	115.9	118.8	-2.6	2.9	0.3
C4-C5-C6	120.6	121.1	119.2	0.4	-1.9	-1.4
C5-C6-C1	119.6	122.2	120.9	2.6	-1.3	1.3
C6-C1-C2	120.4	116.9	120.5	-3.4	3.5	0.1

3.3. Substitution Effect on Ionization Energy

Molecular IE is an important parameter of molecular characteristics. In order to study the effect of fluorine and CN substitutions on ionization energy, we listed the IEs of benzene [54], fluorobenzene [55], benzonitrile [56], 2-fluorobenzonitrile, 3-fluorobenzonitrile, p-fluorobenzonitrile [21], phenol [57], o-fluorophenol [58], m-fluorophenol [59,60] and p-fluorophenol [11] in Table 7, and divided them into four groups for comparison. First, we can find that three molecular IEs reduced with respect to their parent molecules, i.e. for the fluorine substitution, the ionization energy of fluorobenzene, 4-fluorophenol, and 4-fluorobenzonitrile are reduced by 330, 490, and 48 cm^{-1} compared with their parent molecules, respectively, where fluorine plays a role of electron donor. However, fluorine substituted *ortho* and *meta* benzonitrile slightly increased the IEs by 160 and 383 cm^{-1}, respectively; and fluorine substituted *ortho* and *meta* (cis and trans) phenols increased the IEs by 1381, 1563, and 1824 cm^{-1}, respectively. For these substitutions, fluorine exhibits electron withdrawing properties. It can be seen that the role of fluorine changes with the characteristics of parent molecule and different substitution positions. Unlike fluorine substitution, CN substituted benzene and fluorobenzene at *ortho*, *meta*, and *para* positions increase the ionization energy by 3933, 4423, 4646, and 3773 cm^{-1}, respectively, playing a role of strong electron withdrawing.

In addition, we can see from Table 7 that the effects of *ortho* and *meta* substitution on ionization energy are very close, while the effect of *para* substitution is relatively weak. Moreover, the IEs of molecules formed by *ortho*, *meta* and *para* substitutions meets the relative relationship: *para* < *ortho* < *meta*. Most benzene derivative molecules follow this rule.

Table7. Ionization energy of benzene, phenol, and their F and CN substituted molecules (cm^{-1}).

molecule	IE	ΔIE	molecule	IE	ΔIE
Benzene [a]	74557	0	Benzonitrile [c]	78490	0
Fluorobenzene [b]	74227	-330	2-Fluorobenzonitrile [d]	78650	160
Benzonitrile [c]	78490	3933	3-Fluorobenzonitrile [d]	78873	383
			4-Fluorobenzonitrile [e]	78000	-490

 doi:10.20944/preprints202305.2016.v1

Phenol [f]	68625	0			
2-Fluorophenol [g]	70006	1381	Fluorobenzene [b]	74227	0
3-Fluorophenol, cis [h,i]	70188	1563	2-fluorobenzonitrile [d]	78650	4423
3-Fluorophenol, trans [h,i]	70449	1824	3-fluorobenzonitrile [d]	78873	4646
4-Fluorophenol [j]	68577	-48	4-fluorobenzonitrile [e]	78000	3773

[a] Ref. [54]. [b] Ref. [55]. [c] Ref. [56]. [d] This work. [e] Ref. [21]. [f] Ref. [57]. [g] Ref. [58]. [h] Ref. [59,60]. [i] Ref. [60]. [j] Ref. [11].

4. Materials and Methods

4.1 Experimental Methods

The 2-fluorobenzonitrile and 3-fluorobenzonitrile samples were purchased from J&K Chemical and Sigma-Aldrich company, respectively. They were used without further purification. They are colorless or light brown liquid with a purity of 99%. The sample is heated to about 130 °C for 2FBN and 60°C for 3FBN to obtain sufficient vapor pressure. 3 bar krypton for 2FBN and 2.5 bar argon for 3FBN were used as the carrier gases, and they carried the sample molecules into the beam source chamber through a pulse valve of 0.5 mm diameter nozzle (0.8 mm for 3FBN). And then, the molecule beam entered the ionization chamber through a skimmer located 20 mm downstream from the nozzle orifice. The vacuum pressures of the beam source and ionization chambers are ~4×10^{-4} Pa and ~6×10^{-6} Pa, respectively.

The light source consists of two sets of dye lasers pumped by YAG lasers. One dye laser (CBR-D-24, Sirah) pumped by a frequency-tripled Nd: YAG laser (Qsmart 850, Quantel) was used as the excitation laser. Another dye laser (Precision Scan-D, Sirah) pumped by another frequency-tripled Nd: YAG laser (Qsmart 850, Quantel) was used as the ionization laser for two-color REMPI or probe laser for MATI experiments. The dyes of coumarin 540A and coumarin 460 or coumarin 480 were used for the excitation and ionization lasers, respectively. The dye laser wavelengths were calibrated by a wavemeter (WS7-60 UV-I). The fundamental outputs of the dye lasers were further frequency-doubled by BBO crystals.

Due to the strong electron withdrawing ability of the CN group, the transition energies of $S_1 \leftarrow S_0$ are lower than those of $D_0 \leftarrow S_1$ for 2FBN and 3FBN. Such an energy structure indicates that two sets of light sources are required for the measurement of excited state spectra. In the REMPI experiments, we fixed the ionization laser at 232 nm, then scan the excitation laser from 265 to 279 nm to obtain vibronic spectra of the first electronically excited state S_1 for 2FBN and 3FBN.

In the MATI experiments, the molecules in neutral ground state S_0 were resonantly excited to specific vibronic levels in the S_1 state, further excited to the high Rydberg state by the probe laser, which has a scanning range of 224 – 240 nm. A -0.5 V/cm pulsed electric field was applied to remove the prompt ions. After a time delay of about 29 μs, the Rydberg molecules were ionized by a 143 V/cm pulsed electric field. Newly formed threshold ions pass through a 48 cm field-free region to be detected by a Microchannel plates (MCP) detector. The signal was collected by a multichannel scaler (SRS: SR430) and recorded by a computer. Each mass spectrum was accumulated for 300 laser shots. The time sequence of the whole system is controlled by a pulse delay generator (SRS: DG645). More details on the experimental system have been described in our previous publications [61–63].

4.2 Theoretical Methods

All calculations were performed using the Gaussian 16 program package [64]. The geometry optimization, vibrational frequencies of S_0, S_1, and D_0 states are calculated at the levels of RB3LYP/aug-cc-pvtz, TD-B3LYP/aug-cc-pvtz, and UB3LYP/aug-cc-pvtz, respectively. Prior to the experiments, we also using the G4 and CBS-QB3 methods to predict IEs in order to select the appropriate dyes. The spectral simulations are performed based on above B3LYP/aug-cc-pvtz calculations. Combining with the theoretical calculations

 doi:10.20944/preprints202305.2016.v1

and simulated spectra, the vibrational features of 2FBN and 3FBN measured by REMPI and MATI experiments were assigned.

5. Conclusions

The high-resolution vibrational spectra of the first electronically excited state S_1 and cationic ground state D_0 of 2-fluorobenzonitrile and 3-fluorobenzonitrile were measured by two-color resonance enhanced multiphoton ionization and mass analyzed threshold ionization spectroscopy. The precise band origins of $S_1 \leftarrow S_0$ transition and adiabatic ionization energies are determined to be 36028 ± 2 cm^{-1} and 78650 ± 5 cm^{-1} for 2-fluorobenzonitrile; and 35989 ± 2 cm^{-1} and 78873 ± 5 cm^{-1} for 3-fluorobenzonitrile, respectively. DFT theory at the level of B3LYP/aug-cc-pvtz was used to calculate the molecular structure, vibrational frequency, and further perform the Franck-Condon simulations. The theoretical results are in good agreement with the experimental measurements. The vibrational features of S_1 and D_0 states are analyzed in detail and assigned.

The MATI spectra follow well the propensity rule $\Delta v = 0$, indicating that the molecular structures of the cationic ground states are similar to that of the excited states. The molecular structures and vibration frequencies in S_0, S_1, and D_0 states were discussed in detail. The ring C-C bond lengths in S_0, S_1, and D_0 states averagely obey the rule of $S_1 > D_0 > S_0$. The bond length reflects the bond strength, and further the bond length is related with the vibration frequency. On average or for most vibrational modes, the vibration frequencies of the ground state S_0, excited state S_1 and cationic ground state D_0 meet the relative relationship: $S_1 < D_0 < S_0$. At the transition of $S_1 \leftarrow S_0$ and $D_0 \leftarrow S_1$, a lot of vibrational modes associated with ring in-plane distortion were active, and only a few out-of-plane fundamental vibrations were observed. The substitution effects of F and CN were discussed. Whether the electron donating group or the electron withdrawing group, the ionization energies of molecules formed by *ortho*, *meta* and *para* substitutions meet the relative relationship: *para* < *ortho* < *meta*.

Author Contributions: Conceptualization, C.L. and S.J.; investigation, S.L. and Y.Z.; writing—original draft preparation, C.L. and S.L.; writing—review and editing, C.L. and Y.Z.; funding acquisition, Y.J.; J.Z. and S.J. All authors have read and agreed to the published version of the manuscript.

Funding: This research was funded by National Natural Science Foundation of China (Grants Nos. 61835007, 12241408, 61575115), PCSIRT (Grant No. IRT_17R70), 111 project (Grant No. D18001), and the Fund for Shanxi ''1331 Project'' Key Subjects Construction.

Institutional Review Board Statement: Not applicable.

Informed Consent Statement: Not applicable.

Data Availability Statement: The data that support the findings of this study are available from the corresponding author upon reasonable request.

Conflicts of Interest: The authors declare no conflict of interest.

Sample Availability: Samples of 2-fluorobenzonitrile and 3-fluorobenzonitrile are available from commercial sources.

References

1. Berger, R.; Resnati, G.; Metrangolo, P.; Weber, E.; Hulliger, J. ChemInform Abstract: Organic Fluorine Compounds: A Great Opportunity for Enhanced Materials Properties. *ChemInform* **2011**, *42*, no-no, doi:10.1002/chin.201149232.
2. Ametamey, S.M.; Honer, M.; Schubiger, P.A. Molecular imaging with PET. *Chem. Rev.* **2008**, *108*, 1501–1516, doi:10.1021/cr0782426.

3. Müller, K.; Faeh, C.; Diederich, F. Fluorine in pharmaceuticals: looking beyond intuition. *Science* **2007**, *317*, 1881–1886, doi:10.1126/science.1131943.
4. Jeschke, P. The unique role of fluorine in the design of active ingredients for modern crop protection. *Chembiochem* **2004**, *5*, 571–589, doi:10.1002/cbic.200300833.
5. Da Ribeiro Silva, M.A.V.; Monte, M.J.S.; Rocha, I.M.; Cimas, A. Energetic study applied to the knowledge of the structural and electronic properties of monofluorobenzonitriles. *J. Org. Chem.* **2012**, *77*, 4312–4322, doi:10.1021/jo3002968.
6. Ling, F.; Li, S.; Song, X.; Tang, Y.; Wang, Y.; Zhang, B. Visualization of coherent nuclear motion between different geometries in photoexcited 2,4-difluorophenol. *Phys. Rev. A* **2017**, *95*, doi:10.1103/physreva.95.043421.
7. Ling, F.; Wang, Y.; Li, S.; Wei, J.; Tang, Y.; Zhang, B. Imaging Reversible and Irreversible Structural Evolution in Photoexcited 2,4-Difluoroaniline. *J. Phys. Chem. Lett.* **2018**, *9*, 5468–5473, doi:10.1021/acs.jpclett.8b01841.
8. Sun, W.; Lozada, I.B.; van Wijngaarden, J. Fourier Transform Microwave Spectroscopic and ab Initio Study of the Rotamers of 2-Fluorobenzaldehyde and 3-Fluorobenzaldehyde. *J. Phys. Chem. A* **2018**, *122*, 2060–2068, doi:10.1021/acs.jpca.7b11673.
9. Sun, W.; van Wijngaarden, J. Structural elucidation of 2-fluorothiophenol from Fourier transform microwave spectra and ab initio calculations. *Journal of Molecular Structure* **2017**, *1144*, 496–501, doi:10.1016/j.molstruc.2017.05.051.
10. Kamaee, M.; Sun, M.; Luong, H.; van Wijngaarden, J. Investigation of Structural Trends in Mono-, Di-, and Pentafluorobenzonitriles Using Fourier Transform Microwave Spectroscopy. *J. Phys. Chem. A* **2015**, *119*, 10279–10292, doi:10.1021/acs.jpca.5b07379.
11. Zhang, B.; Li, C.; Su, H.; Lin, J.L.; Tzeng, W.B. Mass analyzed threshold ionization spectroscopy of p-fluorophenol cation and the p-fluoro substitution effect. *Chemical Physics Letters* **2004**, *390*, 65–70, doi:10.1016/j.cplett.2004.04.013.
12. Huang, J.; Huang, K.; Liu, S.; Luo, Q.; Tzeng, W. Vibrational spectra and theoretical calculations of p-chlorophenol in the electronically excited S1 and ionic ground D0 states. *Journal of Photochemistry and Photobiology A: Chemistry* **2008**, *193*, 245–253, doi:10.1016/j.jphotochem.2007.07.002.
13. Ratzer, C.; Nispel, M.; Schmitt, M. Structure of 4-fluorophenol and barrier to internal –OH rotation in the S1-state. *Phys. Chem. Chem. Phys.* **2003**, *5*, 812–819, doi:10.1039/b210188b.
14. Zhang, L.; Liu, S.; Cheng, M.; Du, Y.; Zhu, Q. Vibrational Spectra and Theoretical Calculations of cis- and trans-3-Fluoro-N-methylaniline in the Neutral (S(0)) and Cationic (D(0)) Ground States. *J. Phys. Chem. A* **2016**, *120*, 81–94, doi:10.1021/acs.jpca.5b11991.
15. Arivazhagan, M.; Meenakshi, R.; Prabhakaran, S. Vibrational spectroscopic investigations, first hyperpolarizability, HOMO-LUMO and NMR analyzes of p-fluorobenzonitrile. *Spectrochim. Acta A Mol. Biomol. Spectrosc.* **2013**, *102*, 59–65, doi:10.1016/j.saa.2012.09.070.
16. Da Ribeiro Silva, M.A.V.; Monte, M.J.S.; Rocha, I.M.; Cimas, A. Energetic study applied to the knowledge of the structural and electronic properties of monofluorobenzonitriles. *J. Org. Chem.* **2012**, *77*, 4312–4322, doi:10.1021/jo3002968.
17. Varadwaj, P.R.; Jaman, A.I. Centrifugal distortion analysis of the millimeter-wave spectrum of 2-fluorobenzonitrile and ab initio DFT calculations. *Journal of Molecular Spectroscopy* **2006**, *236*, 70–74, doi:10.1016/j.jms.2005.12.009.
18. Kumar, A.P.; Rao, G.R. Vibrational analysis of substituted benzonitriles. I. Vibrational spectra, normal coordinate analysis and transferability of force constants of monohalogenated benzonitriles. *Spectrochim. Acta A Mol. Biomol. Spectrosc.* **1997**, *53A*, 2023–2032, doi:10.1016/S1386-1425(97)00131-5.
19. Palmer, M.H.; Moyes, W.; Spiers, M. The electronic structure of substituted benzenes: ab initio calculations and photoelectron spectra for benzonitrile, the tolunitriles, fluorobenzonitriles, dicyanobenzenes and ethynylbenzene. *Journal of Molecular Structure* **1980**, *62*, 165–187, doi:10.1016/0022-2860(80)85234-3.
20. Jiang, S.; Levy, D.H. Supersonic Jet Studies on the Photophysics of Substituted Benzenes and Naphthalenes. *J. Phys. Chem. A* **2002**, *106*, 8590–8598, doi:10.1021/jp025764a.

21. Zhao, Y.; Jin, Y.; Hao, J.; Yang, Y.; Li, C.; Jia, S. Resonance enhanced multiphoton ionization and mass analyzed threshold ionization spectroscopy of 4-fluorobenzonitrile. *Chemical Physics Letters* **2018**, *711*, 127–131, doi:10.1016/j.cplett.2018.09.039.
22. Eom, S.Y.; Lee, Y.R.; Kwon, C.H. Accurate conformational stability and cationic structure of piperidine determined by conformer-specific VUV-MATI spectroscopy. *Phys. Chem. Chem. Phys.* **2020**, *22*, 22823–22832, doi:10.1039/d0cp04407e.
23. Park, S.M.; Lee, Y.R.; Kwon, C.H. Conformational Structures of Neutral and Cationic Pivaldehyde Revealed by IR-Resonant VUV-MATI Mass Spectroscopy. *Int. J. Mol. Sci.* **2022**, *23*, doi:10.3390/ijms232314777.
24. Lee, Y.R.; Kwon, C.H. Valence molecular orbitals and cationic structures of 2-fluoropyridine by high-resolution ion spectroscopy and Franck-Condon fitting. *J. Chem. Phys.* **2022**, *157*, 154306, doi:10.1063/5.0119832.
25. Lee, Y.R.; Kwon, C.H. Innovative mass spectrometer for high-resolution ion spectroscopy. *J. Chem. Phys.* **2021**, *155*, 164203, doi:10.1063/5.0066348.
26. Eom, S.Y.; Lee, Y.R.; Park, S.M.; Kwon, C.H. Determination of the highest occupied molecular orbital and conformational structures of morpholine based on its conformer-specific photoionization dynamics. *Phys. Chem. Chem. Phys.* **2022**, *24*, 28477–28485, doi:10.1039/d2cp04112j.
27. Eom, S.Y.; Kang, D.W.; Kwon, C.H. Conformational structure of cationic tetrahydropyran by one-photon vacuum ultraviolet mass-analyzed threshold ionization spectroscopy. *Phys. Chem. Chem. Phys.* **2021**, *23*, 1414–1423, doi:10.1039/d0cp05969b.
28. Lee, Y.R.; Kim, H.L.; Kwon, C.H. Determination of the cationic conformational structure of tetrahydrothiophene by one-photon MATI spectroscopy and Franck-Condon fitting. *Phys. Chem. Chem. Phys.* **2020**, *22*, 6184–6191, doi:10.1039/d0cp00073f.
29. Kang, D.W.; Yoon, D.K.; Kwon, C.H. Conformational potential energy surfaces and cationic structure of 3,4-dihydro-2H-pyran by VUV-MATI spectroscopy and Franck-Condon fitting. *Phys. Chem. Chem. Phys.* **2020**, *22*, 27673–27680, doi:10.1039/d0cp05193d.
30. Ketkov, S.Y.; Tzeng, S.-Y.; Rychagova, E.A.; Markin, G.V.; Makarov, S.G.; Tzeng, W.-B. Laser spectroscopic and computational insights into unexpected structural behaviours of sandwich complexes upon ionization. *Dalton Trans.* **2021**, *50*, 10729–10736, doi:10.1039/d1dt01887f.
31. Ketkov, S.; Tzeng, S.-Y.; Rychagova, E.; Tzeng, W.-B. Ionization of Decamethylmanganocene: Insights from the DFT-Assisted Laser Spectroscopy. *Molecules* **2022**, *27*, doi:10.3390/molecules27196226.
32. Ketkov, S.Y.; Tzeng, S.Y.; Rychagova, E.A.; Kalakutskaya, L.V.; Fuss, M.; Braunschweig, H.; Tzeng, W.-B. Rydberg state mediated multiphoton ionization of (η7-C7H7)(η5-C5H5)Cr: DFT-supported experimental insights into the molecular and electronic structures of excited sandwich complexes. *Phys. Chem. Chem. Phys.* **2019**, *21*, 9665–9671, doi:10.1039/c9cp00888h.
33. Ketkov, S.Y.; Rychagova, E.A.; Tzeng, S.-Y.; Tzeng, W.-B. TD DFT insights into unusual properties of excited sandwich complexes: structural transformations and vibronic interactions in Rydberg-state bis(η6-benzene)chromium. *Phys. Chem. Chem. Phys.* **2018**, *20*, 23988–23997, doi:10.1039/c8cp04845b.
34. Ketkov, S.Y.; Tzeng, S.-Y.; Wu, P.-Y.; Markin, G.V.; Tzeng, W.-B. DFT-Supported Threshold Ionization Study of Chromium Biphenyl Complexes: Unveiling the Mechanisms of Substituent Influence on Redox Properties of Sandwich Compounds. *Chemistry* **2017**, *23*, 13669–13675, doi:10.1002/chem.201702226.
35. Ketkov, S.Y.; Markin, G.V.; Tzeng, S.Y.; Tzeng, W.B. Fine Substituent Effects in Sandwich Complexes: A Threshold Ionization Study of Monosubstituted Chromium Bisarene Compounds. *Chemistry* **2016**, *22*, 4690–4694, doi:10.1002/chem.201505039.
36. Tzeng, S.Y.; Takahashi, K.; Tzeng, W.B. Two-Color Resonant Two-Photon Mass-Analyzed Threshold Ionization of 2,4-Difluoroanisole and the Additivity Relation of Ionization Energy. *J. Phys. Chem. A* **2020**, *124*, 10517–10526, doi:10.1021/acs.jpca.0c08272.
37. Kemp, D.J.; Whalley, L.E.; Tuttle, W.D.; Gardner, A.M.; Speake, B.T.; Wright, T.G. Vibrations of the p-chlorofluorobenzene cation. *Phys. Chem. Chem. Phys.* **2018**, *20*, 12503–12516, doi:10.1039/c8cp01274a.
38. Davies, A.R.; Kemp, D.J.; Wright, T.G. Electronic, vibrational, and torsional couplings in N-methylpyrrole: Ground, first excited, and cation states. *J. Chem. Phys.* **2021**, *154*, 224305, doi:10.1063/5.0050654.

39. Kemp, D.J.; Gardner, A.M.; Tuttle, W.D.; Midgley, J.; Reid, K.L.; Wright, T.G. Identifying complex Fermi resonances in p-difluorobenzene using zero-electron-kinetic-energy (ZEKE) spectroscopy. *J. Chem. Phys.* **2018**, *149*, 94301, doi:10.1063/1.5045544.
40. Davies, A.R.; Kemp, D.J.; Wright, T.G. Comment on "Electronic, vibrational and torsional couplings in N-methylpyrrole: Ground, first excited and cation states" J. Chem. Phys. 154, 224305 (2021). *J. Chem. Phys.* **2021**, *155*, 117101, doi:10.1063/5.0063264.
41. Kemp, D.J.; Fryer, E.F.; Davies, A.R.; Wright, T.G. Vibration-modified torsional potentials and vibration-torsion ("vibtor") levels in the m-fluorotoluene cation. *J. Chem. Phys.* **2019**, *151*, 84311, doi:10.1063/1.5116520.
42. Davies, A.R.; Kemp, D.J.; Warner, L.G.; Fryer, E.F.; Rees, A.; Wright, T.G. Variations in Duschinsky rotations in m-fluorotoluene and m-chlorotoluene during excitation and ionization. *J. Chem. Phys.* **2020**, *152*, 214303, doi:10.1063/5.0009391.
43. Varsányi, G. *Assignments for vibrational spectra of seven hundred benzene derivatives;* Adam Hilger: London, 1974, ISBN 0852742835.
44. Wilson, E.B. The Normal Modes and Frequencies of Vibration of the Regular Plane Hexagon Model of the Benzene Molecule. *Phys. Rev.* **1934**, *45*, 706–714, doi:10.1103/physrev.45.706.
45. Asmis, K.R.; Yang, Y.; Santambrogio, G.; Brümmer, M.; Roscioli, J.R.; McCunn, L.R.; Johnson, M.A.; Kühn, O. Gas-phase infrared spectroscopy and multidimensional quantum calculations of the protonated ammonia dimer N2H7+. *Angew. Chem. Int. Ed Engl.* **2007**, *46*, 8691–8694, doi:10.1002/anie.200702607.
46. Yang, Y.; Kuhn, O. A concise method for kinetic energy quantisation. *Mol. Phys.* **2008**, *106*, 2445–2457, doi:10.1080/00268970802562117.
47. Davies, A.R.; Kemp, D.J.; Wright, T.G. Unpicking vibration-vibration and vibration-torsion interactions in m-fluorotoluene. *Journal of Molecular Spectroscopy* **2021**, *381*, 111522, doi:10.1016/j.jms.2021.111522.
48. Tzeng, S.Y.; Takahashi, K.; Tzeng, W.B. Two-Color Resonant Two-Photon Mass-Analyzed Threshold Ionization of 2,4-Difluoroanisole and the Additivity Relation of Ionization Energy. *J. Phys. Chem. A* **2020**, *124*, 10517–10526, doi:10.1021/acs.jpca.0c08272.
49. Xu, Y.; Tzeng, S.Y.; Shivatare, V.; Takahashi, K.; Zhang, B.; Tzeng, W.B. Identification of four rotamers of m-methoxystyrene by resonant two-photon ionization and mass analyzed threshold ionization spectroscopy. *J. Chem. Phys.* **2015**, *142*, 124314, doi:10.1063/1.4916052.
50. Xu, Y.; Tzeng, S.Y.; Zhang, B.; Tzeng, W.B. Rotamers of 3,4-difluoroanisole studied by two-color resonant two-photon mass-analyzed threshold ionization spectroscopy. *Spectrochim. Acta A Mol. Biomol. Spectrosc.* **2013**, *102*, 365–370, doi:10.1016/j.saa.2012.10.020.
51. Huang, W.C.; Huang, P.S.; Hu, C.H.; Tzeng, W.B. Vibronic and cation spectroscopy of 2,4-difluoroaniline. *Spectrochim. Acta A Mol. Biomol. Spectrosc.* **2012**, *93*, 176–179, doi:10.1016/j.saa.2012.03.015.
52. Shivatare, V.S.; Kundu, A.; Patwari, G.N.; Tzeng, W.B. Studies of structural isomers o-, m-, and p-fluorophenylacetylene by two-color resonant two-photon mass-analyzed threshold ionization spectroscopy. *J. Phys. Chem. A* **2014**, *118*, 8277–8286, doi:10.1021/jp501059c.
53. Li, C.; Lin, J.L.; Tzeng, W.B. Mass-analyzed threshold ionization spectroscopy of the rotamers of p-n-propylphenol cations and configuration effect. *J. Chem. Phys.* **2005**, *122*, 44311, doi:10.1063/1.1839863.
54. Neuhauser, R.G.; Siglow, K.; Neusser, H.J. High n Rydberg spectroscopy of benzene: Dynamics, ionization energy and rotational constants of the cation. *J. Chem. Phys.* **1997**, *106*, 896–907, doi:10.1063/1.473170.
55. Lembach, G.; Brutschy, B. Fragmentation energetics and dynamics of fluorobenzene · Arn (n=1–3) clusters studied by mass analyzed threshold ionization spectroscopy. *J. Chem. Phys.* **1997**, *107*, 6156–6165, doi:10.1063/1.474281.

56. Araki, M.; Sato, S.; Kimura, K. Two-Color Zero Kinetic Energy Photoelectron Spectra of Benzonitrile and Its van der Waals Complexes with Argon. Adiabatic Ionization Potentials and Cation Vibrational Frequencies. *J. Phys. Chem.* **1996**, *100*, 10542–10546, doi:10.1021/jp960565a.
57. Dopfer, O.; Müller-Dethlefs, K. S1 excitation and zero kinetic energy spectra of partly deuterated 1:1 phenol–water complexes. *J. Chem. Phys.* **1994**, *101*, 8508–8516, doi:10.1063/1.468111.
58. Yuan, L.; Li, C.; Lin, J.L.; Yang, S.C.; Tzeng, W.B. Mass analyzed threshold ionization spectroscopy of o-fluorophenol and o-methoxyphenol cations and influence of the nature and relative location of substituents. *Chemical Physics* **2006**, *323*, 429–438, doi:10.1016/j.chemphys.2005.10.004.
59. Oikawa, A.; Abe, H.; Mikami, N.; Ito, M. Electronic spectra and ionization potentials of rotational isomers of several disubstituted benzenes. *Chemical Physics Letters* **1985**, *116*, 50–54, doi:10.1016/0009-2614(85)80123-8.
60. Yosida, K.; Suzuki, K.; Ishiuchi, S.; Sakai, M.; Fujii, M.; Dessent, C.E.H.; Müller-Dethlefs, K. The PFI-ZEKE photoelectron spectrum of m-fluorophenol and its aqueous complexes: Comparing intermolecular vibrations in rotational isomers. *Phys. Chem. Chem. Phys.* **2002**, *4*, 2534–2538, doi:10.1039/b201107g.
61. Zhao, Y.; Jin, Y.; Hao, J.; Yang, Y.; Wang, L.; Li, C.; Jia, S. Rotamers of p-isopropylphenol studied by hole-burning resonantly enhanced multiphoton ionization and mass analyzed threshold ionization spectroscopy. *Spectrochim. Acta A Mol. Biomol. Spectrosc.* **2019**, *207*, 328–336, doi:10.1016/j.saa.2018.09.013.
62. Li, N.; Li, S.; Wang, L.; Wang, H.; Zhao, J.; Li, C. Vibrational spectra of 2-cyanophenol cation studied by the mass analyzed threshold ionization technique. *Chemical Physics Letters* **2022**, *792*, 139402, doi:10.1016/j.cplett.2022.139402.
63. Hao, J.; Duan, C.; Yang, Y.; Li, C.; Jia, S. Resonance enhanced two-photon ionization and mass analyzed threshold ionization spectroscopy of 4-ethylanisole. *Journal of Molecular Spectroscopy* **2020**, *369*, 111258, doi:10.1016/j.jms.2020.111258.
64. Frisch, M.J.; Trucks, G.W.; Schlegel, H.B.; Scuseria, G.E.; Robb, M.A.; Cheeseman, J.R.; Scalmani, G.; Barone, V.; Mennucci, B.; Petersson, G.A.; et al. Gaussian 16; Gaussian Inc.: Wallingford, CT, USA, 2016.